

Sussex Research

Charge-tunnelling and self-trapping: common origins for blinking, grey-state emission and photoluminescence enhancement in semiconductor quantum dots

Mark Osborne, Aidan Fisher

Publication date

07-05-2016

Licence

This work is made available under the [CC BY 4.0](#) licence and should only be used in accordance with that licence. For more information on the specific terms, consult the repository record for this item.

Document Version

Published version

Citation for this work (American Psychological Association 7th edition)

Osborne, M., & Fisher, A. (2016). *Charge-tunnelling and self-trapping: common origins for blinking, grey-state emission and photoluminescence enhancement in semiconductor quantum dots* (Version 1). University of Sussex. <https://hdl.handle.net/10779/uos.23429087.v1>

Published in

Nanoscale

Link to external publisher version

<https://doi.org/10.1039/C6NR00529B>

Copyright and reuse:

This work was downloaded from Sussex Research Open (SRO). This document is made available in line with publisher policy and may differ from the published version. Please cite the published version where possible. Copyright and all moral rights to the version of the paper presented here belong to the individual author(s) and/or other copyright owners unless otherwise stated. For more information on this work, SRO or to report an issue, you can contact the repository administrators at sro@sussex.ac.uk. Discover more of the University's research at <https://sussex.figshare.com/>

Supplementary Information

Charge-tunnelling and self-trapping: common origins for blinking, grey-state emission and photoluminescence enhancement in semiconductor quantum dots

*Mark A. Osborne^{*a} and Aidan Fisher^a*

^aDepartment of Chemistry, School of Life Sciences, University of Sussex, Falmer, Brighton,
BN1 9QJ, UK. Email: m.osborne@sussex.ac.uk

Note S1. Kinetics and steady-state approximations.

A number of approximations to the simulation algorithm have been made to reduce computational times without compromising the resolution of the key properties observed in QD photoluminescence (PL) trajectories. Firstly it assumed that sampling of the QD core and surface by the exciton-hole occurs rapidly (ps) compared to radiative recombination (ns). The carrier surface-state is therefore not explicitly included in the stochastic simulation, but instead steady-state an equilibrium constant between the surface and core state, k_h^+/k_h^- modulate the exciton-state population, where k_h^+ and k_h^- are forward (+) and back (-) tunnelling rate constants to and from the QD surface. Assuming that electron ionisation to the external trap (k_h^+) and recovery (k_h^-) is slow compared to radiative (k_r) and non-radiative (k_{nr}) relaxation and applying the steady-state

approximation, then the algorithm is reduced to three key transition rates; the PL rate, r_{rad} ; the electron loss rate (QD-to-host), r_{ion} and the return rate, r_{rec} , given by

$$\begin{aligned}
 r_{\text{rad}} &= k_r f_c \\
 r_{\text{ion}} &= k_i^+ (f_c + f_s) \quad \text{where} \\
 r_{\text{rec}} &= k_i^-
 \end{aligned}
 \quad
 \begin{aligned}
 f_c &= \frac{k_x k_h^-}{k_h^- (k_r + k_{\text{nr}}) + k_x (k_h^- + k_h^+)} \\
 f_s &= \frac{k_x k_h^+}{k_h^- (k_r + k_{\text{nr}}) + k_x (k_h^+ + k_h^-)}
 \end{aligned}
 \tag{S1}$$

where k_x is the excitation rate and f_c the core exciton-fraction, which is modulated by the exciton-hole sampling the surface with fraction f_s . Here, the core-exciton fraction is emissive in the neutral-state with a radiative rate constant k_r , while the hole-surface fraction is assumed not to undergo radiative relaxation due to localisation and reduced wavefunction overlap with the core exciton-electron. Tunnelling of the electron to the external host-trap is assumed independent of hole-location and electron recovery from the trap is independent of the QD-state. The model is made quantitative by parameterizing the tunnelling rate constants, k_h^+ , k_h^- , k_i^+ and k_i^- in terms of physical properties of the system, namely barrier heights and tunnelling distances. Information supporting the definition of these parameters is provided in the following sections.

Note S2. The capture cross-section

The tunnelling rate constants k_h^+ , k_h^- , k_i^+ and k_i^- are defined to first order within the WKB approximation to the tunnelling probability. For a particle of mass, m with kinetic energy, E and a potential-barrier of height, V , the probability of tunnelling a length, l , is given by, $\exp(-l\sqrt{8m(V-E)}/\hbar)$. Here, we assume the tunnelling lengths differ for the lighter, exciton-

electron and heavier, localised hole. In the simplest model, the exciton-hole tunnels only to the QD surface and the tunnelling length l is replaced by a “fixed” distance, $d = R_s - R_c$, defining the shell thickness, where R_c and R_s are the QD-core and core + shell radii. For the electron, there will be a range of accessible distances dependent on the distribution of traps in the host. Assuming electron-traps are distributed uniformly throughout the host-material, then tunnelling lengths from the QD to the trap are sampled from a distribution that is uniform in the interval between 0 and some maximum tunnelling length, l_{\max} , defined here by the characteristic Bjerrum length, the threshold at which the electron at thermal energy can escape the electrostatic attraction of the charged-QD, $kT = e^2/\epsilon_{\text{QD}}l_{\max}$ (Gaussian units), where ϵ_{QD} is the dielectric constant of the QD.

Assuming a uniform distribution of traps in the host medium surrounding the QD, the trap density will increase with the radial distance R_0 from the QD centre as, $N = 4\pi R_0^2$, such that the capture probability ($N\sigma/4\pi R_0^2$) for the outbound electron is dependent only on the trap cross-section $\sigma = \pi r^2$, where r is the trap radius (Fig. S2a). In contrast, an electron returns from the trap to a single QD and the probability of capture is proportional to the solid angle subtended at the trap, by either the QD-core ($\sigma = \pi R_c^2$) or a localised hole trapped at the QD-surface, which we assume for simplicity has the dimensions of the same order or magnitude as the electron trap. The solid angle of capture is determined by the distance between the trap and recombination centres. For forward-tunnelling from and back-tunnelling to the QD-core this is given by

$$R_0 = R_s + r_h + l + r_e \quad (\text{S2})$$

where l is the tunnelling length, r_e and r_h are the radii of the host-electron and QD surface-hole traps respectively. For back-tunnelling to the QD surface, the cosine rule is used to give

$$R_0^2 = (R_s + r_h + l + r_e)^2 + (R_s + r_h)^2 - 2(R_s + r_h + l + r_e)(R_s + r_h) \cos \theta \quad (\text{S3})$$

The centre-to-centre distance is then dependent on the angle θ , subtended by QD-to-electron and QD-to-hole vector. In principle, the hole can be found trapped at any site on the surface with θ randomised accordingly using, $\cos \theta = 2u - 1$, where u is a random number in $[0,1]$ (Fig. S2b). Interestingly, we find the kinetics are best described by a sufficiently narrow range of θ , that the problem can be represented by a simple 1D tunnelling coordinate, with a centre-to-centre distance between the host-trapped electron and the excess-hole on the QD reduced to $R_0 = r_h + l + r_e$.

Note S3. The mean tunnelling barrier

For the tunnelling-barrier we represent the potential by the arithmetic mean of the barrier-heights from the initial and final-states, which differ for tunnelling processes from and to the QD valence band (VB) and conduction band (CB) edge and the host-trap and QD surface-states. The mean-barrier is a reasonable approximation for an arbitrary potential where large barriers and tunnelling distances combine to give an exponent $l\sqrt{(V - E)} \geq 4$, for a free electron mass m_0 , l in Å and V and E in eV.¹ For $E_{\text{ea}} > 4.5$ eV (CdSe), stabilisation energies $\phi_e \sim 2$ eV, kinetic confinement energies, $E \sim 0.5$ eV and a free electron mass, the condition is readily met for tunnelling distances $l > 2.3$ Å. Given QD blinking times measured in the range 10^{-3} - 10^3 s correspond to distances > 7 Å, the mean-barrier approximation would appear valid in this case. Note, for the electron ionised to the host-trap, the rate constant depends also on the probability of tunnelling through the QD

shell with thickness, d and barrier height, $\phi_{\text{CB}} \sim 1.46$ eV, defined by the CdSe-core to ZnS-shell conduction band-offset.

Note S4. Charge-carrier trap energetics

The QD-surface trap for the excess hole is defined by simple electrostatics, by assuming the charge-carrier is stabilised by its image at the host-QD interface. The trap depth, in this case, is defined by the self-energy, $\phi_{\text{h}} = (1/\epsilon_{\text{s}} - 1/\epsilon_{\text{QD}}) K e^2 / 2r_{\text{h}}$, above the QD-VB edge, where r_{h} is the hole-trap dimension and $K = (\epsilon_{\text{QD}} - \epsilon_{\text{s}}) / (\epsilon_{\text{QD}} + \epsilon_{\text{s}})$ is a screening factor due to the dielectric mismatch between the QD and the surface medium, with dielectric constant ϵ_{QD} and ϵ_{s} respectively. The self-energy is classically unbounded at the interface and r_{h} is a cut-off imposed to regularise the potential, such that the trap is represented by a linear extrapolation of the potential within a “lattice-spacing” either side of the interface.² The environment surrounding the QD is strictly a composite of surface-passivating ligands and the support medium such that the dielectric constant, ϵ_{s} at the QD-host interface will differ from that in the host, away from the QD. We account for inclusion of the ligand into the host material using the Maxwell-Garnett effective medium approximation³, for which the dielectric constant is given below along with the size dependent QD static dielectric constant ϵ_{QD} ⁴

$$\epsilon_{\text{s}} = \epsilon_{\text{m}} \frac{2\delta(\epsilon_{\text{lig}} - \epsilon_{\text{m}}) + \epsilon_{\text{lig}} + 2\epsilon_{\text{m}}}{\delta(\epsilon_{\text{m}} - \epsilon_{\text{lig}}) + \epsilon_{\text{lig}} + 2\epsilon_{\text{m}}} \quad (\text{S4})$$

$$\epsilon_{\text{QD}} = 1 + \frac{\epsilon_{\text{bulk}} - 1}{1 + (0.75 / 2R_{\text{c}})^{1.2}}$$

where δ is the fractional contribution of the ligand to the effective dielectric constant at the QD surface, ϵ_{lig} is the dielectric constant of the ligand and ϵ_{bulk} the dielectric constant of bulk CdSe making up the QD-core. Bulk ZnS does not differ significantly in dielectric constant and the core dielectric constant is assumed uniform throughout the QD core and shell for simplicity. Inclusion of a surface-ligand contribution to the host dielectric is motivated by an observed sensitivity of on-time blinking statistics to ligand exchange,⁵ but it was also found necessary in our simulation to reproduce the narrow spread of α_{on} values across the different QD-support media.

Definition of the external, host electron-trap energy ϕ_e is motivated by the dielectric dependence of the on and off-blinking kinetics. We assume the tunnelling-electron is stabilised in the host by simple solvation with an energy, $\phi_e = (1 - 1/\epsilon_m) e^2/2r_e$, below the QD-CB edge, where ϵ_m is the dielectric constant of the QD-host medium and r_e defines the size of the solvation cavity. In general, the macroscopic dielectric properties of the medium will be well known. On the other hand, the size of the self-trapping cavity is a local, microscopic property, dependent on the nature of the defect and structural rearrangement of the host about the solvated charge. Deep trapping requires the charge-carrier to be localised at a vacancy or interstitial with dimensions on the order of the lattice spacing, typically several Angstroms. For example, *p*-terphenyl has a lattice constant of 0.56 nm in the smallest dimension⁶, while the less ordered amorphous SiO₂ has a dominant interstitial void size of 0.6 nm diameter⁷ and PVA has an average unit cell dimension of 0.53 nm.⁸ Here, we use a cavity radius of 0.3 nm to normalise cavity size effects and focus on the dielectric dependence of blinking.

Note S5. Exciton-carrier confinement energetics

In principle, the kinetic energies of the exciton-electron and hole, $E_{e(h)}$, can be calculated from a correct “particle-in-a-box” description of the exciton-pair under confinement. In its simplest form the “box” is spherical and the potential infinite at the walls, but such a model tends to inaccuracy for small, structured nanocrystals with finite ionisation potentials. Here, we exploit the empirical relationship between the first exciton transition energy of the QD and radius to derive kinetic energies (Fig. S3).⁹ We find the transition energy (eV) is well represented by the simple functional form, $E_{\text{QD}} = 1.9 + 0.8R_c^2$, where R_c is the QD core radius (nm) in the range 1-3 nm. The energy of the exciton-pair at the band-edge, E_x and component electron and hole energies, $E_{e(h)}$, are then given by

$$\begin{aligned} E_x &= E_{\text{QD}} - E_g - E_C \\ E_{e(h)} &= \frac{m_{h(e)}}{m_e + m_h} E_x \end{aligned} \tag{S5}$$

where E_g is the bulk band-gap (~ 1.74 eV for CdSe) and $E_C = -1.8e^2/\epsilon_{\text{QD}}R_c$ is the Coulomb potential of the confined exciton-pair.

Note S6. Excitation, Radiative and Auger recombination rates

An empirical relationship between QD extinction coefficient and the radius is used to determine the excitation cross-section, σ_x on which the excitation rate $k_x = \sigma_x \lambda I / hc$ depends, where λ is the excitation wavelength. The absorption cross-section at the first exciton is given in our model by⁹

$$\sigma_x = 1600 E_{\text{QD}} (2R_c)^3 \times \frac{1000 \ln 10}{N_A} \quad (\text{S6})$$

where N_A is Avagadro's number. For simplicity, extrapolation to the excitation wavelength is performed using a parabolic approximation to the absorption profile of the QD at energies higher than the first exciton and by an exponential decay at energies lower than the first exciton.

The spontaneous emission rate also exhibits a QD size dependency. Here we use a simple linear relationship between the radiative rate k_r (ns^{-1}) and the emission energy E_{em} (eV) that has recently been reported in the literature¹⁰

$$k_r = 0.0753E_{\text{em}} - 0.1151 \quad (\text{S7})$$

Assuming PL is dominated by near band-edge emission ($E_{\text{em}} \sim E_{\text{QD}}$), then a QD of radius $R_c = 2$ nm ($E_{\text{QD}} = 2.1$ eV) has a radiative relaxation time of $k_r^{-1} = 23$ ns.

Incorporating further size dependent properties, we adopt a carrier-density dependent Auger recombination rate $C_A(N/V)^2$, where N/V is the electron-hole pair density and C_A is the Auger constant, which for CdSe QDs has been shown to hold a R_c^3 dependency with a constant of proportionality of approximately $10^{-30} \text{ cm}^6\text{s}^{-1}$.¹¹ Given the carrier density is dependent on the QD volume, the overall dependency of the non-radiative Auger relaxation rate is given by

$$k_{\text{nr}} = 9 \times 10^{-30} N^2 / (16\pi^2 R_c^3 \times 10^{-42}) \quad (\text{S8})$$

For a QD with $R_c = 2$ nm the scaling gives an Auger relaxation time for $N = 2$ electron-hole pairs of $k_{nr}^{-1} = 35$ ps.

Note S7. CTST model input parameters

The CTST model is explicitly parameterised in terms of properties of the QD-host system and therefore provides genuine physical insight into PL processes. However since many of these properties have simple size dependent relationships, either empirically measured or theoretically derived, model input data is minimised. The inputs and the parameters they determine are listed below:

R_c : the QD-core radius, since this ultimately determines rate constants k_x , k_r , k_{nr} , the charge carrier kinetic energies E and the core dielectric constant ϵ_{QD} that determines the exciton-pair Coulomb energy.

R_s : the QD-surface radius is determined by inputs of the lattice spacing of the QD-shell material and the number of monolayers. This determines the exciton-hole tunnelling distance $d = R_s - R_c$ as well as capture-probabilities since centre-to-centre tunnelling distances, R_0 , are dependent of R_s . It also determines the probability p of finding the QD in the core-charged or surface-charged state following ionisation through the surface-to-core ratio of atoms.

ϵ_m (ϵ_s): the host (ligand) dielectric constant (and fill factor) determine self-trap energies, ϕ_e and ϕ_h and the barrier for exciton-hole tunnelling V_{2h}^{\pm} .

r : the trap radius controls the host-electron and QD surface-hole self-trap depth as well as the capture cross-sections $\sigma = \pi r^2$, centre-to-centre electron-tunnelling distance, R_0 and electron-hole recombination probability in quenching of the excess surface-hole state of the ionised QD.

E_g and E_{ea} : the band-gap and electron affinity (bulk CB-edge) of the QD-core material, determine kinetic energies E and, along with self-trapping energies, electron-tunnelling barrier heights, V_{ion}^+ , V_{on}^- , V_{off}^- .

ϕ_{VB} and ϕ_{CB} : valence band and conduction band-offsets of the QD-shell material determine barrier heights for exciton-hole tunnelling between QD core and surface and through shell electron-tunnelling respectively. The former process modulates PL intensities of the neutral and surface-charged, radiative states, while the latter modulates ionisation of the QD with shell thickness d .

I and λ : the excitation intensity and wavelength determine the excitation rate k_x along with the size dependent excitation cross-section).

T : the temperature determines the maximum tunnelling length through the Onsager relationship between thermal energy and the ion-electron Coulomb interaction. The truncation rate, Γ , is also weakly dependent on temperature through an Arrhenius term.

ϕ_D and f : the detection efficiency and excess noise, simulate experimental parameters which are determined from microscope lens, filter and camera specifications.

Simulations of CdSe-ZnS QDs in different dielectric host-media (Fig. S4) were performed with a core radius of $R_c = 2.0$ nm, emitting at $\lambda_{em} = 590$ nm with a 2 monolayer (ML) cap of depth $d = 0.62$ nm, defined by the ZnS lattice spacing. The excitation cross-section $\sigma_x = 1.72 \times 10^{-15}$ cm² (Equation S6), intensity $I = 45$ Wcm⁻² and wavelength $\lambda = 473$ nm define the excitation rate, $k_x = 1.85 \times 10^5$ s⁻¹ and the radiative lifetime is $k_r^{-1} = 23$ ns (Equation S7). The dark-state is governed by a non-radiative Auger relaxation constant of $k_{nr} = 7.13 \times 10^9$ s⁻¹ (Equation S8). The CB-edge of bulk CdSe of -4.95 eV, the band-gap, $E_g = 1.74$ eV and the ZnS band offsets, eV $\phi_{VB} = -0.53$ eV below and $\phi_{CB} = 1.46$ eV above respective CdSe band-edges, were taken from

literature sources, along with the dielectric constants of the host and QD-surface ligands.¹² The temperature was set at $T = 300\text{K}$ and a detection efficiency, $\phi_D = 1\%$, (including photon to ADU gray-scale conversion) an excess noise factor, $f = 1.6$ and a photon integration time $t_{\text{int}} = 80\text{ ms}$ were used to simulate optical characteristics and ICCD imaging settings.

Note S8. The exciton-hole equilibrium constant

Within a pre-exponential constant the rate constants k_h^+ and k_h^- for exciton-hole tunnelling to and from the QD-surface respectively, are given by $k_h^\pm \propto \exp(-d\sqrt{\phi_{\text{VB}} \mp q\phi_{2h}})$, where d is the shell thickness, ϕ_{VB} is the valence band offset, q is the excess charge on the QD and ϕ_{2h} is the sum repulsion between two holes in the valence band. The equilibrium constant for the exciton-hole tunnelling process, $X_{01}^+ \leftrightarrow X_{01}^{+h}$, in the ionised QD with excess-charge at the surface can be approximated by a first order Taylor expansion ($\sqrt{1+x} = 1 + x/2 \dots$) of the tunnelling exponent by making the substitution, $x = \phi_{2h}/\phi_{\text{VB}}$, wherein the equilibrium constant, $k_h^+/k_h^- = \exp(d\sqrt{\phi_{\text{VB}} + \phi_{2h}} - d\sqrt{\phi_{\text{VB}} - \phi_{2h}})$ becomes

$$\frac{k_h^+}{k_h^-} \propto \exp[d(1 + \phi_{2h}/2\phi_{\text{VB}})\phi_{\text{VB}}^{1/2} - d(1 - \phi_{2h}/2\phi_{\text{VB}})\phi_{\text{VB}}^{1/2}] \quad (\text{S9})$$

$$\frac{k_h^+}{k_h^-} \propto \exp(d\phi_{2h}\phi_{\text{VB}}^{-1/2})$$

Evidently the equilibrium constant increases exponentially with decreasing shell thickness, shifting the equilibrium from the quenched surface exciton-hole state, X_{01}^{+h} , back to the emissive

core exciton-hole state, X_{01}^+ . The process provides a mechanism for PL enhancement within the CTST model of blinking and grey-states.

Note S9. The PL intensity trajectory of thick-shelled CdSe/CdS QDs

To demonstrate effect of shell thickness on the PL intensity trajectory and to highlight the versatility of the CTST model we synthesised core/shell CdSe/CdS QDs with a relatively thick 2 monolayer shell using a procedures reported elsewhere.¹³ Briefly CdO (30 mg, 99.5%), stearic acid (0.25g, 95% reagent grade) and 1-Octadecene (ODE, 4mL, 90% technical grade) were heated in a round bottom flask (RBF) to 250°C under N₂ to form a clear, colourless Cd-stearate precursor. The solution was cooled to room temperature, octadecylamine (1.5g, 90% technical grade) added to the flask and the flask heated back to 270°C. A premade selenium precursor solution of Se (0.157g, 99.999%, Alfa Aesar, UK) dissolved in trioctylphosphine (2 mL, 90% technical grade, Acros Organics) was rapidly injected into the hot Cd solution at 270°C and the temperature reduced to 250°C for crystal growth. The reaction was stopped by removal from heat and the nanocrystals were purified by repeated precipitation using methanol and dispersal in hexane. Core CdSe QDs were stored in hexane prior to capping. All chemicals were sourced from Sigma-Aldrich unless stated otherwise.

The CdS shell was grown using the successive ionic layer adsorption and reaction (SILAR) technique.¹³ A Cd-oleate precursor solution (0.1 M) was prepared by dissolving CdO (0.1g) in ODE (6mL) and oleic acid (2.3 mL, 90% technical grade) under N₂ at 250°C. The clear and colourless solution kept at 100°C under N₂ until required. The sulphur precursor (0.1 M) was prepared by dissolving S (0.02g, >99.5%) in ODE (6 mL) at 175°C under N₂. The clear, colourless solution kept at room temperature until required. An RBF was charged with ODA (0.6g), ODE (6 mL) and CdSe core QDs in hexane (3 mL ~ 10⁻⁸ moles). The flask was pumped down for 30

minutes to remove the hexane solvent and then heated to 100°C for a further 10 minutes. After placing under N₂ the flask was heated to 238°C for shell growth. Successive drop wise injections were carried out at 10 minute intervals using pre-calculated shell precursor volumes for the required number of MLs. Following shell growth the reaction mixture was allowed to cool to RT and the QDs purified by repeated precipitation and dispersal using methanol and hexane. Finally core/shell QDs were stored in hexane prior to imaging.

Imaging of the QDs was performed on unmodified glass (SiOx) coverslips using a TIRF microscope with laser excitation 473 nm and 0.08 kWcm⁻² and PL detection on an ICCD camera via a 609 ± 27 nm bandpass filter. PL from QDs was recorded at an integration time of 0.1 s per frame for up to 2500 frames and the PL intensity trajectory from individual QDs in the movie-stack were extracted as the mean intensity within a 5×5 pixel ROI containing each QD (Fig. S5a).

Simulations of the PL intensity trajectory were performed using the CTST within a standard stochastic simulation algorithm. Input parameters were selected to match experimental conditions as closely as possible with a QD size ($R_c = 1.5$ nm and $R_s = 2.2$ nm) based on the measured wavelength of the first exciton peak absorption (Fig. S5a inset) and lattice spacing of a CdS (0.36 nm) cap.¹⁴ The VB (-0.66 eV) and CB (0.0 eV) band-offsets were adjusted to reflect the near-match of the core and shell conduction-band energies for a CdS cap. Ionization of the QD was also made dependent on biexciton formation by modifying the ionization rate constant k_{ion} (Equation S1) to include the probability of generating a second exciton within the radiative lifetime, $r_{ion} = k_i^+ k_x (f_c + f_s)/k_r$. Preliminary data from correlations between the propensity for “grey”-states in QDs and quality of the shell in TEM images, suggest ionization via single-exciton or biexciton mechanisms may be dependent on the structural integrity of the cap and is subject to current investigation. PL intensity trajectory simulations with 2.5 and 3 ML CdS caps (Fig. S5b

and S5c) demonstrate the increasing modulation depth of the grey-state intensity with shell thickness and match closely the experimental data representing an estimated 2 ML CdS capped CdSe. Furthermore, intensity histograms from the experimental PL trajectory and the simulation show clear resolution of the core-charged, dark-state X_{10}^+ population, the surface-charged, “grey”-state X_{01}^+ population, as well as the bright, largely neutral state X_{00} population (Fig. S5d, S5e and S5f).

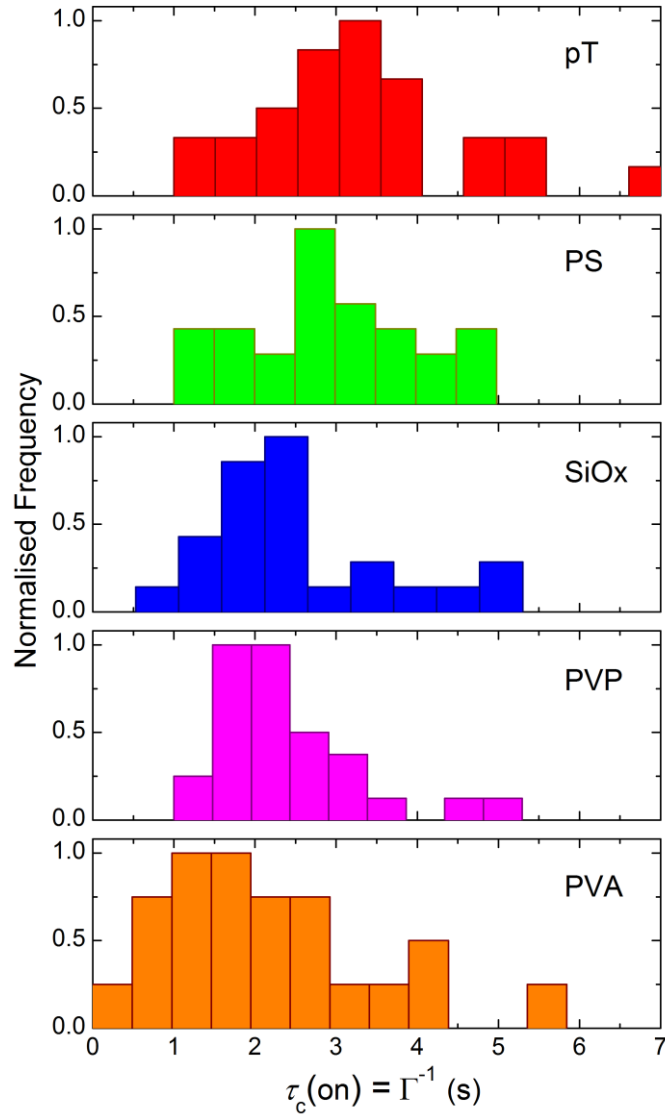


Fig. S1. Dielectric dependence of the cut-off time in the on-time PDD. Truncation times ($\tau_c = \Gamma^{-1}$) obtained from fitting the truncated power law (TPL) to experimentally derived PDDs for CdSe-ZnS QDs (Lumidot 590, Sigma-Aldrich, UK) in *p*-terphenyl (pT, $\epsilon_m = 2.12$), polystyrene (PS, $\epsilon_m = 2.53$), glass (SiOx, $\epsilon_m = 3.8$), poly(N-vinylpyrrolidone, $\epsilon_m = 4.8$) (PVP) and polyvinylalcohol (PVA, $\epsilon_m = 14$).

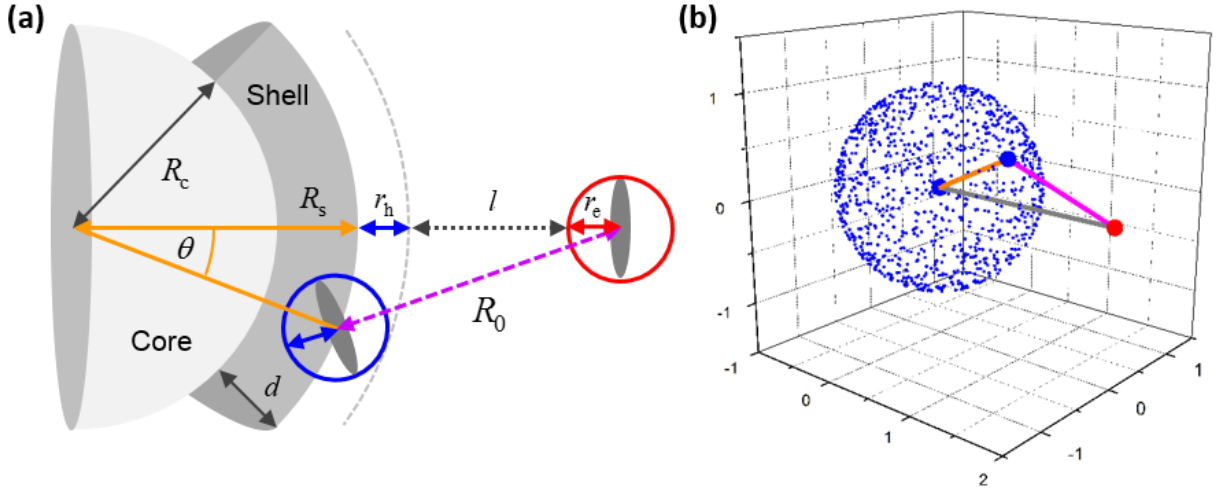


Fig. S2. Geometry of the CTST model. (a) Definition of the capture cross-section. The host electron-trap (red) radius r defines a capture cross-section $\sigma = \pi r^2$ and probability of capture proportional to the solid angle $\sigma/4\pi R_0^2$ subtended at the QD centre, where R_0 is the electron and hole, centre-to-centre distance. For the electron returning to X_{10}^+ , the QD presents a cross-section of radius R_c , while recombination in X_{01}^+ takes place at a localised hole trapped (blue) at the QD surface where R_0 is defined by the cosine rule (Equation S3). (b) Distribution of hole sites (blue) represent single QD-to-surface tunnelling events. Electron tunnelling coordinate, defined by the QD centre-to-trap (grey), QD centre-to-surface hole (orange) and hole-to-electron vectors (magenta).

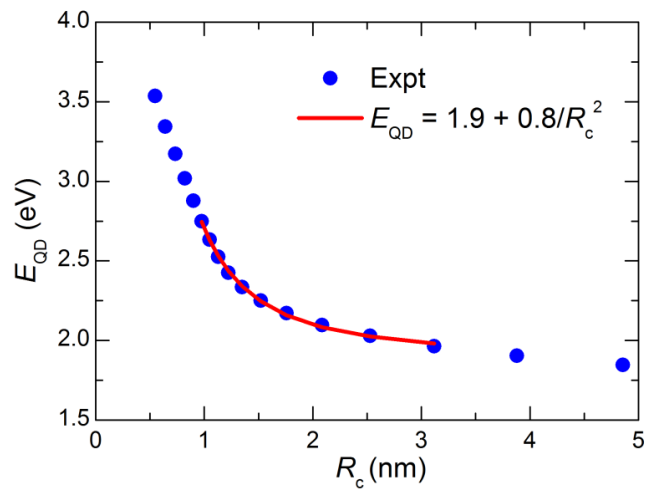


Fig. S3. First exciton energy versus QD core-radius for CdSe. Experimental data points are derived from ref. [9] and the curve is the best fit of $A + B/R_c^2$, with $A = 1.9$ and $B = 0.8$.

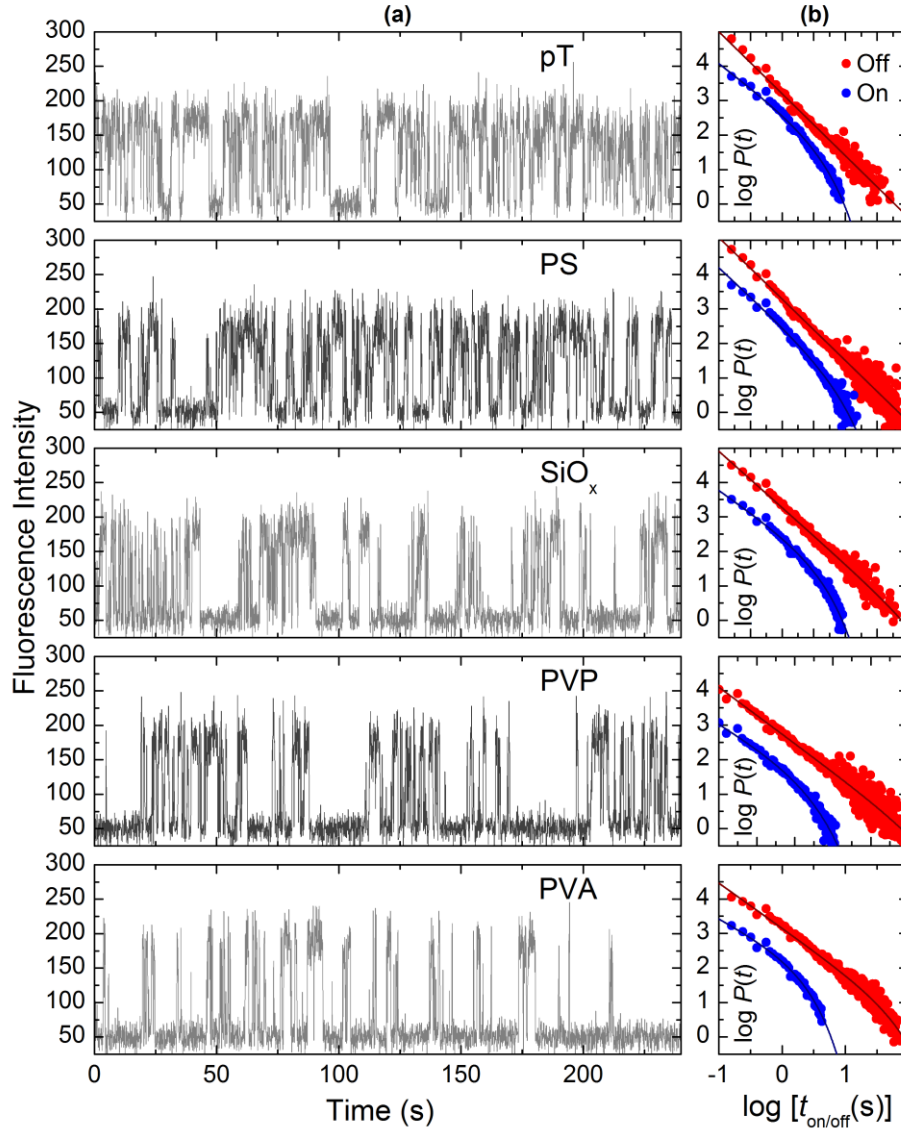


Fig. S4. Simulated single QD PL intensity trajectories and blinking statistics. (a) Extracts from PL trajectories for CdSe-ZnS QDs in media of different dielectric constants: pT ($\epsilon_m = 2.12$), PS ($\epsilon_m = 2.53$), SiO_x ($\epsilon_m = 3.8$), PVP ($\epsilon_m = 4.8$) and PVA ($\epsilon_m = 14$). Full trajectories contain more than 2500 on/off switching events and typically cover observations times of 1000-3000 s depending on the dielectric constant. (b) Log-log on-time and off-time PDDs averaged from over 20 simulated trajectories (>50000 events) for each host-medium along with corresponding fits of the TPL to each PPD. The trend from mostly PL on to largely PL off with increasing ϵ_m is quantitatively comparable to experiment (Fig. 1a). CTST model in input parameters are matched closely to experimental conditions (Note S7).

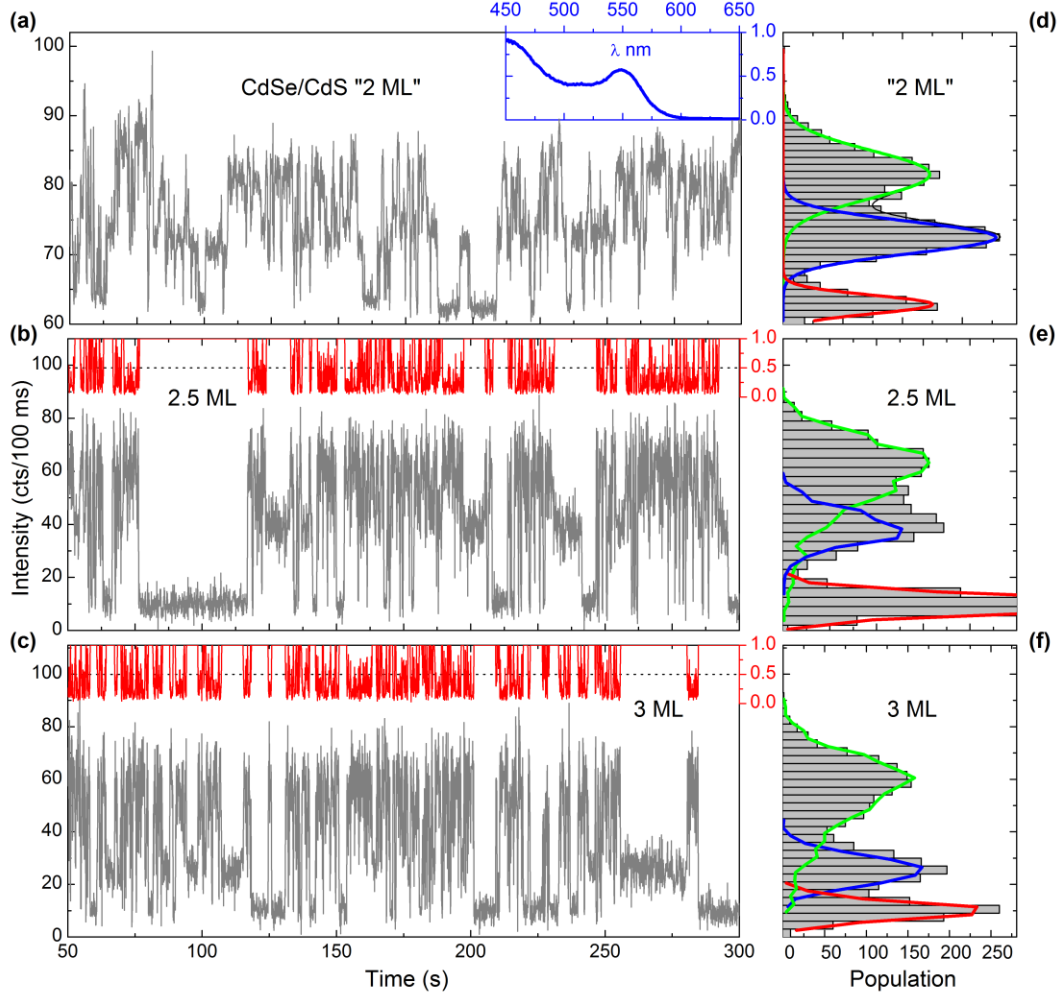


Fig. S5. Resolution of the dark, “grey” and bright states in thick-shelled QDs. (a) Experimental PL intensity trajectory of synthesised CdSe/CdS QD on glass (SiOx) with an estimated 2-3 ML CdS cap (from TEM). Absorption spectrum of the synthesised QD stock (inset blue) with first exciton peak $\lambda = 550$ nm corresponding to a core diameter ~ 3 nm.⁹ (b) Simulated PL intensity trajectory for a CdSe/CdS QD with a core size $R_c = 1.5$ and 2.5 ML CdS cap ($R_s = 1.5 + 2.5 \times 0.36 = 2.22$ nm). Host-matrix and QD-surface dielectric constants were fixed at $\epsilon_m = 3.8$ (SiOx) and $\epsilon_s = 2$ (TOP) respectively. (c) As for (B) but for 3 ML CdS cap. (d) Intensity histogram derived from the PL trajectory in (a) showing resolution of the dark (red), “grey” (blue) and bright (green) states. Fitted normal distributions are for guidance only since core, surface and net charge on the QD is not tracked experimentally. (e) and (f) Intensity histograms derived from simulations (b) and (c) showing the change in depth of the intensity modulation and contributions from core-charged X_{10}^+ (red), surface-charged X_{01}^+ (blue) and mixed states $X_{01}^+ + X_{10}^+ + X_{00}$ (green) with cap thickness.

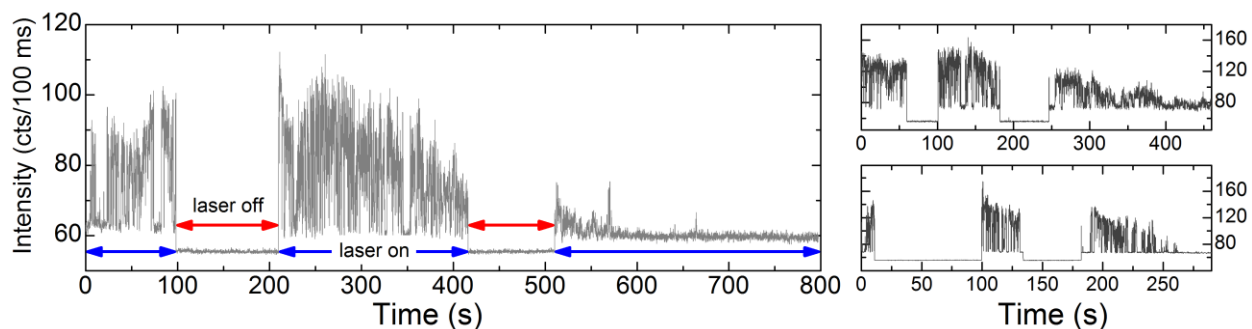


Fig. S6. PL enhancement (PE) and decay with intermittent CW illumination. Experimental intensity envelope of PE and photobleaching of single ZnS capped CdSe (Lumidot 590) QDs on glass (SiO_x) under intermittent excitation at 473 nm. Periods of paused illumination (laser off) varied from 50 to 100 s with QDs typically resuming emission levels and continued PE and decay following the recommencement of continuous excitation (laser on). Reversible PE and darkening of PL during periods of non-illumination was evident in our PE experiments.

Host	ϵ_m	α_{on}	τ_c (on)	α_{off}	τ_c (off)
pT	2.12	1.46 ± 0.16	3.29	1.75 ± 0.08	89 ± 23
PS	2.53	1.44 ± 0.13	2.74	1.71 ± 0.07	98 ± 28
SiOx	3.8	1.40 ± 0.14	2.38	1.60 ± 0.05	99 ± 34
PVP	4.8	1.39 ± 0.10	1.96	1.57 ± 0.07	106 ± 30
PVA	14	1.17 ± 0.15	1.46	1.45 ± 0.08	79 ± 36

Table S1. Exponents and cut-off times obtained from experimental PL intensity trajectories simulations of CdSe-ZnS QDs in different dielectric host media. Exponents $\alpha_{on/off}$ and τ_c (on/off) obtained from fitting the TPL to on- and off-time PDDs generated from experimental PL intensity trajectories. Errors in represent α_{on} , α_{off} and τ_c (off) standard deviations in the data set of more the 25 QDs per dielectric host. Values of τ_c (on) represent peak values from broad distributions of cut-off rates (Fig. S1).

Host	ϵ_m	ϕ_e (eV)	ϵ_s	ϕ_h (eV)	V_{ion}^+ (eV)	V_{on}^- (eV)	V_{off}^- (eV)
pT	2.12	1.27	2.52	0.38	4.32	5.99	5.80
PS	2.53	1.45	2.65	0.35	4.22	6.25	6.08
SiOx	3.8	1.77	3.0	0.26	4.06	6.69	6.56
PVP	4.8	1.90	3.26	0.22	3.99	6.86	6.75
PVA	14	2.23	5.40	0.04	3.83	7.27	7.25

Table S2. Stabilisation energies and mean tunnelling barrier heights in the CTST model for a CdSe QD as a function of host dielectric constant ϵ_m . Values are for $R_c = 2$ nm, $r = 0.3$ nm, $\epsilon_{QD} = 8.9$ and a ligand dielectric constant 2.7 (HDA)¹² and fill factor $\delta = 0.7$ used in the effective medium approximation of the dielectric constant at the QD surface, ϵ_s (Eqn. S4).

Host	ϵ_m	on			off		
		$\alpha_{\text{on}} (\text{fit})$	$\tau_c (\text{fit})$	$\tau_c (\text{CTST})$	$\alpha_{\text{off}} (\text{fit})$	$\tau_c (\text{fit})$	$\tau_c (\text{CTST})$
pT	2.12	1.43 ± 0.08	3.3	3.4	1.79 ± 0.08	150	58
PS	2.53	1.44 ± 0.16	3.1	3.1	1.76 ± 0.06	138	58
SiOx	3.8	1.31 ± 0.09	2.7	2.6	1.61 ± 0.05	117	58
PVP	5.3	1.24 ± 0.14	2.2	2.3	1.55 ± 0.04	79	57
PVA	14	1.00 ± 0.14	1.5	1.3	1.32 ± 0.05	49	45

Table S3. Exponents and cut-off times obtained from PL intensity trajectory simulations of CdSe-ZnS QDs in different dielectric host media. Exponents $\alpha_{\text{on/off}}$ and $\tau_c (\text{fit})$ obtained from fitting the TPL to on- and off-time PDDs generated from simulated PL intensity trajectories. $\tau_c (\text{CTST})$ obtained directly from model Equation 3 (main article). Simulations were performed for CdSe core size $R_c = 2 \text{ nm} + 2 \text{ ML shell} \times 0.31 \text{ nm}$ ZnS lattice spacing gives $R_s = 2.62 \text{ nm}$ with other parameters as defined for Fig. 3 (main article) and Fig. S4. Note $\tau_c (\text{fit})$ for on-times are subject to uncertainties of $\sim 30\%$. For off-times, values for $\tau_c (\text{fit})$ represent averages from simulations with finite values of τ_c falling between 0 and the simulation length of 3000s. Off-time truncations show the correct order of magnitude, but are subject to uncertainties of $>100\%$ due to limited events arising from stochastic simulations at long times.

References

1. K. H. Gundlach and J. G. Simmons, *Thin Solid Films*, 1969, **4**, 61-79.
2. L. Banyai, P. Gilliot, Y. Z. Hu and S. W. Koch, *Phys. Rev. B*, 1992, **45**, 14136-14142.
3. J. C. M. Garnett, *Philos T R Soc Lond*, 1904, **203**, 385-420.
4. L. W. Wang and A. Zunger, *Phys. Rev. B*, 1996, **53**, 9579-9582.
5. A. Issac, C. Krasselt, F. Cichos and C. von Borczyskowski, *ChemPhysChem*, 2012, **13**, 3223-3230.
6. G. W. Bak, *J Phys C Solid State*, 1987, **20**, 1129-1136.
7. M. Hasegawa, M. Saneyasu, M. Tabata, Z. Tang, Y. Nagai, T. Chiba and Y. Ito, *Nuc. Instr. Meth. Phys. Res. B*, 2000, **166**, 431-439.
8. C. W. Bunn, *Nature*, 1948, **161**, 929-930.
9. W. W. Yu, L. H. Qu, W. Z. Guo and X. G. Peng, *Chem. Mater.*, 2003, **15**, 2854-2860.
10. C. D. Donega and R. Koole, *J. Phys. Chem. C*, 2009, **113**, 6511-6520.
11. V. I. Klimov, A. A. Mikhailovsky, D. W. McBranch, C. A. Leatherdale and M. G. Bawendi, *Science*, 2000, **287**, 1011-1013.
12. W. M. Haynes, *CRC Handbook of Chemistry and Physics, 95th Edition*, CRC Press, 2014.
13. R. G. Xie, U. Kolb, J. X. Li, T. Basche and A. Mews, *J. Am. Chem. Soc.*, 2005, **127**, 7480-7488.
14. O. Chen, J. Zhao, V. P. Chauhan, J. Cui, C. Wong, D. K. Harris, H. Wei, H. S. Han, D. Fukumura, R. K. Jain and M. G. Bawendi, *Nat. Mater.*, 2013, **12**, 445-451.